

Cross-section measurements in the NOMAD experiment

R. Petti^{ab *†}

^a CERN, CH-1211 Genève 23, Switzerland

^b University of South Carolina, Columbia SC 29208, USA

The NOMAD experiment collected valuable neutrino data samples, matching both the large statistics of massive calorimeters and the reconstruction quality of bubble chambers. This paper describes the recent measurements of neutrino cross-sections on carbon target. The approach followed for cross-section modeling is also explained.

1. Introduction

The NOMAD experiment was designed to search for ν_τ appearance from neutrino oscillations in the CERN wide-band neutrino beam produced by the 450 GeV proton synchrotron. The single-particle reconstruction and lepton identification capability of the NOMAD detector allowed the search for ν_τ appearance in most of the leptonic and hadronic τ decay channels [1] and also to look for $\nu_\mu \rightarrow \nu_e$ oscillations [2]. No evidence for oscillations was found.

The high resolution and reconstruction quality makes the NOMAD data samples a valuable resource for the neutrino physics community. The recent measurements of cross-sections and particle production would help to clarify our understanding of neutrino interactions with nuclei at intermediate energies. In addition, it must be noted the precise tracking in a light target provides a powerful tool to tune and validate Monte Carlo simulation programs for future experiments. This analysis activity can benefit from the beam and detector studies performed for the oscillation searches.

2. Detector and data samples

The NOMAD detector is described in detail in Ref. [3]. Inside a 0.4 T magnetic field there is an active target consisting of drift chambers (DC) [4] with a fiducial mass of about 2.7 tons

and a low average density (0.1 g/cm³). The main target, 405 cm long and corresponding to about one radiation length, is followed by a transition radiation detector (TRD) [5] for electron identification, a preshower detector (PRS), and a high resolution lead-glass electromagnetic calorimeter (ECAL) [6]. A hadron calorimeter (HCAL) and two stations of drift chambers for muon detection are located just after the downstream part of the magnet coil. An iron-scintillator sampling calorimeter with a fiducial mass of about 17t (FCAL) is located upstream of the central part of the NOMAD target. The detector is designed to identify leptons and to measure muons, pions, electrons and photons with comparable resolutions. Momenta are measured in the DC with a resolution:

$$\frac{\sigma_p}{p} \simeq \frac{0.05}{\sqrt{L[m]}} \oplus \frac{0.008 \times p[\text{GeV}/c]}{\sqrt{L[m]^5}}$$

where L is the track length and p is the momentum. The energy of electromagnetic showers, E , is measured in the ECAL with a resolution:

$$\frac{\sigma_E}{E} = 0.01 \oplus \frac{0.032}{\sqrt{E[\text{GeV}]}}.$$

The relative composition of Charged Current (CC) events in NOMAD is estimated [7] to be $\nu_\mu, \bar{\nu}_\mu, \nu_e, \bar{\nu}_e = 1.00 : 0.0227 : 0.0154 : 0.0016$, with average neutrino energies of 45.4, 40.8, 57.5, and 51.5 GeV, respectively. Neutrinos are produced at an average distance of 625 m from the detector.

*For the NOMAD collaboration

†E-mail address: Roberto.Petti@cern.ch

The NOMAD experiment collected data from 1995 to 1998. Most of the running, for a total exposure of 5.1×10^{19} protons on target (pot), was in neutrino mode. This resulted in three distinct data samples, according to the different targets: $1.3 \times 10^6 \nu_\mu$ CC interactions from the drift chambers (mainly carbon), $1.5 \times 10^6 \nu_\mu$ CC interactions from the region of the magnet coil (mainly aluminium) located in front of the DC and $1.2 \times 10^7 \nu_\mu$ CC interactions from FCAL (iron).

3. Modeling of inelastic cross-sections

3.1. Structure functions at high Q^2

At large momentum transfer structure functions are described as series in Q^{-2} on the basis of the operator product expansion of the correlator of the weak current (twist expansion):

$$F_i(x, Q^2) = F_i^{\text{TMC}}(x, Q^2) + \frac{H_i^{(4)}(x)}{Q^2} + \frac{H_i^{(6)}(x)}{Q^4} + \dots, \quad (1)$$

where $i = T, 2, 3$ refers to the type of the structure function, F_i^{TMC} are the leading twist (LT) terms corrected for the target mass effects and $H_i^{(t)}$ are the higher twist (HT) terms of twist t . The target mass corrections are computed using the approach of Ref.[8] (see also [11] for the treatment of the threshold problem at $x \rightarrow 1$). The calculation of the leading twist is performed in the NNLO approximation and we include additional phenomenological terms up to twist-6. We use PDFs and HT based on Ref.[9], obtained from dedicated fits optimized at low Q^2 [10] and including additional data from (anti)neutrinos CC (NOMAD, CHORUS [25] and NuTeV [24]) and charged lepton (JLab) Deep Inelastic Scattering (DIS), as well as from Drell-Yan production (E605 and E886).

3.2. Low Q^2 structure functions

In the low- Q region (anti)neutrino cross sections are dominated by the longitudinal structure function F_L and the latter is driven by the axial-current interactions. The structure function F_T vanishes as Q^2 at low Q^2 . This behaviour is similar to the charged lepton case and holds

for both the vector and the axial-vector contributions. However, in the longitudinal channel the low- Q behavior of the vector and axial-vector parts are different.

The conservation of the vector current (CVC) suggests $q_\mu W_{\mu\nu} = 0$ for the vector current part of hadronic tensor. From this condition we conclude F_L^V vanishes faster than F_T^V at low Q^2 and $F_L^V/F_T^V \sim Q^2$. This behavior is similar to the charged-lepton case.

In contrast to the vector current, the axial-vector current is not conserved. For low momentum transfer the divergence of the axial-vector current is proportional to the pion field (Partially Conserved Axial Current or PCAC)

$$\partial A^\pm = f_\pi m_\pi^2 \varphi^\pm. \quad (2)$$

where m_π is the pion mass and $f_\pi = 0.93m_\pi$ is the pion decay constant and φ^\pm is the pion field in the corresponding charge state. We introduce explicitly a PCAC contribution to F_L^A :

$$F_L^A = \gamma^3 F_L^{\text{PCAC}} f_{\text{PCAC}}(Q^2) + \tilde{F}_L^A \quad (3)$$

where $\gamma = (1 + 4x^2 M^2/Q^2)^{1/2}$, $F_L^{\text{PCAC}} = f_\pi^2 \sigma_\pi/\pi$ and $\sigma_\pi = \sigma_\pi(s, Q^2)$ is the total cross section for the scattering of a virtual pion with momentum q and the center-of-mass energy squared $s = (p + q)^2$. The last term \tilde{F}_L^A is similar to F_L^V and vanishes as Q^4 . Since the PCAC contribution is expected to vanish at high Q^2 we introduce a form factor $f_{\text{PCAC}}(Q^2) = (1 + Q^2/M_{\text{PCAC}}^2)^{-2}$, where the dipole form is motivated by meson dominance arguments. It is important to note the pion pole does not directly contribute to structure functions and hence the mass scale controlling the PCAC mechanism, M_{PCAC} , cannot be the pion mass itself, but is rather related to higher mass states like $a_1, \rho\pi$ etc. We use the simple assumption $M_{\text{PCAC}} = m_{a_1}$ [12].

The structure functions F_T and $\tilde{F}_L = F_L^V + \tilde{F}_L^A$, which are vanishing for $Q^2 \rightarrow 0$ like in the charged lepton case, are parameterized as smooth interpolations between the high Q^2 regime calculated from Equation 1 and the $Q^2 \rightarrow 0$ predictions derived from current conservation arguments [10][13]. We choose the value $Q_0^2 = 1 \text{ GeV}^2$ as matching point for the twist expansion. In the

region $0 < Q^2 < 1 \text{ GeV}^2$ we use cubic splines calculated for fixed x values. The coefficients of such functions are fully determined by the condition both functions and derivatives should match with the twist expansion at Q_0^2 . Figure 1 illustrates the interpolation procedure for F_2 on protons in charged lepton scattering.

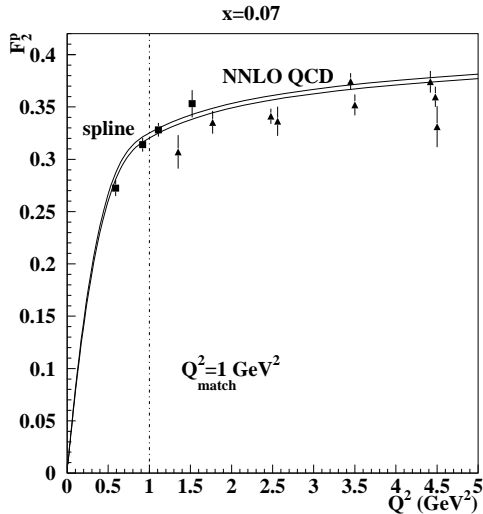


Figure 1. Interpolation of structure functions in the region $0 < Q^2 < 1 \text{ GeV}^2$. The example given in the plot refers to F_2 for charged lepton scattering on protons at $x=0.07$ (see text for details).

The different Q^2 dependence of various terms in Equation 1 allows to disentangle higher twist contributions, which are parameterized as smooth functions (splines) of x . Our results indicate the twist-6 term $\propto 1/Q^4$ is important in order to describe the ratio R of longitudinal to transverse cross-sections at low Q^2 . This is shown in Figure 2 together with SLAC and JLab data. We derive the ratio R directly from the parameterizations of F_L and F_T .

From the relation $F_2 = (F_L + F_T)/\gamma^2$ and (3) it follows that the structure function F_2 at low Q^2

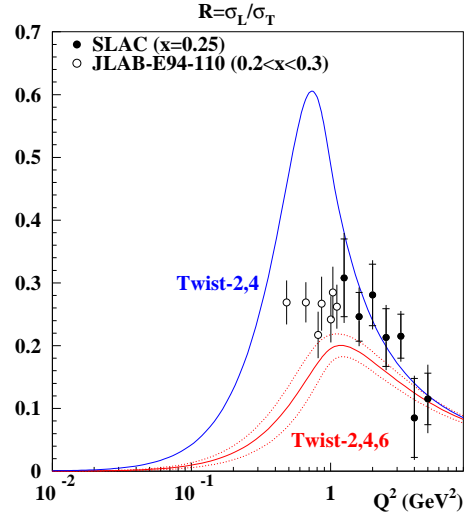


Figure 2. Impact of higher twist terms on $R = \sigma_L/\sigma_T$ for charged lepton scattering. Data from SLAC and JLab are shown for comparison.

is dominated by the nonvanishing F_L^{PCAC} term (Figure 3). It is important to note that since $F_T \rightarrow 0$ and $F_L \rightarrow F_L^{\text{PCAC}}$ in the limit of vanishing Q^2 the ratio $R = F_L/F_T$ is divergent for neutrino interactions. This is substantially different from the scattering of charged leptons for which R is vanishing as Q^2 .

The determination of LT and HT terms is performed from all available data with $Q^2 > 0.5 \text{ GeV}^2$ and $W > 1.9 \text{ GeV}$. It is interesting to check the extrapolation of DIS structure functions into the resonance region. The results are consistent with the duality principle, as can be seen from Figure 4 where the integral of the difference between the recent JLab resonance data and the average DIS predictions is consistent with zero.

3.3. Nuclear and electroweak corrections

A detailed calculation of nuclear corrections to structure functions is performed [11][14]. The model takes into account a number of different

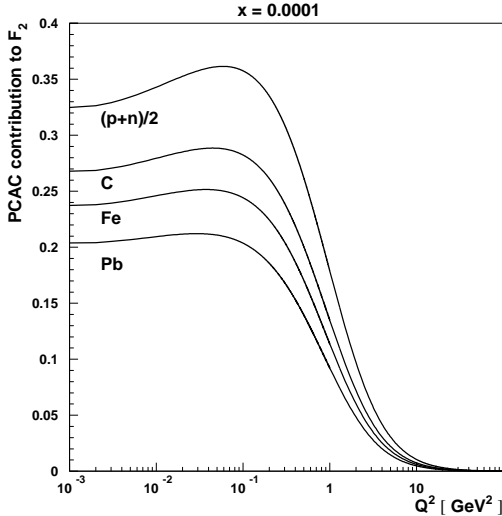


Figure 3. The PCAC contribution to the neutrino structure function F_2 at $x = 10^{-4}$ for different targets.

effects including nuclear shadowing, Fermi motion and binding, nuclear pion excess and off-shell correction to bound nucleon structure functions. The off-shell effect and the effective scattering amplitude describing nuclear shadowing are expressed in terms of few parameters which are common to all nuclei and have a clear physical interpretation. The parameters are then extracted from statistical analysis of data from charged lepton scattering on a wide range of nuclear targets.

The treatment of Fermi motion, binding, off-shell effect and nuclear pion correction in (anti)neutrino interactions is similar to the one in charged lepton scattering. The main differences are related to the impact of the axial-vector current on coherent nuclear effects and are more evident at low Q^2 [14].

One-loop electroweak effects are taken into account [15] as corrections to the parton distributions used in the structure function calculation. The initial quark mass singularities from QED corrections are subtracted within the $\overline{\text{MS}}$

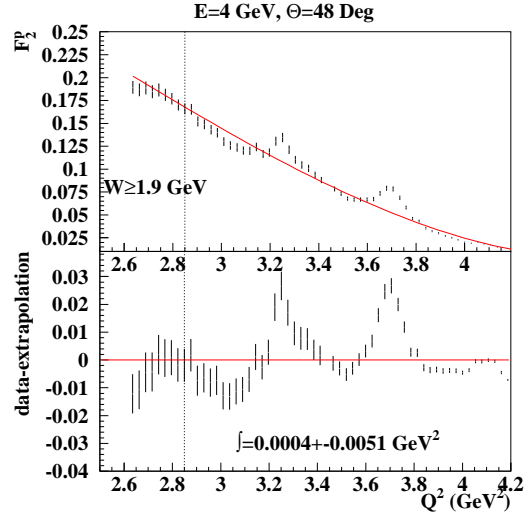


Figure 4. Comparison between the extrapolation of DIS F_2 structure function on proton and the recent JLab data in the resonance region.

scheme since they are effectively incorporated in the quark density functions. Results are cross-checked with a second independent calculation [16].

3.4. Neutrino fluxes

Two independent approaches are used to calculate neutrino fluxes. The first method is based on a simulation of the West Area Neutrino Facility [7]. The calculation of particle production rates from the interaction of primary protons on Be target is performed with a recent version of FLUKA [17], further modified to take into account the cross-sections measured by the SPY and NA20 experiments. These particles are then propagated through the beam line taking into account the material and magnetic fields they traverse. Predictions are then validated by comparisons with NOMAD data.

A second method relies directly upon the ν_μ CC events reconstructed in the NOMAD detector. In particular, events with low energy associated to

the hadronic system ($\nu < 3$ GeV) are analyzed to this purpose since the corresponding differential distribution $dN/d\nu$ is proportional to the flux up to a small correction factor ($\sim 10\%$).

3.5. Monte Carlo simulations

The Monte Carlo (MC) simulation of neutrino DIS interactions is based on LEPTO 6.1 [18] and JETSET 7.4 [19] packages, followed by a full GEANT3 [20] propagation to model the detector response. The neutrino cross-sections are parameterized according to the model described in the previous Sections. The simulation of resonance production is performed according to Ref. [21].

We do not include the parton shower treatment from JETSET. The reinteractions of hadrons with surrounding nucleons in target nuclei are described within the DPMJET [22] package. A detailed tuning of fragmentation parameters has been performed with hadrons reconstructed in ν_μ CC interactions [23].

4. Measurement of inelastic cross-section

The present knowledge of neutrino cross-sections is rather nonuniform. In the region $E_\nu > 30$ GeV, where data from the large massive calorimeters (CCFR, NuTeV) are available, the uncertainty is about 2%. This increases to about 20% at lower energies, due to the limited statistics of bubble chamber experiments. Measurements of both the total σ_{CC}^{tot} and the differential $d\sigma_{CC}^2/dxdy$ cross-sections for ν_μ on carbon are performed in NOMAD. One of the primary goals is to constrain the (anti)neutrino cross-section model and to reduce the corresponding systematic uncertainties. This also provides the first measurement of inclusive cross-section on carbon target, with $\langle Q^2 \rangle \sim 13$ GeV².

The absolute normalization is obtained from the world average cross-section on isoscalar target in the energy range $40 < E_\nu < 300$ GeV. The measurement is performed in the kinematic region $\nu > 3$ GeV and $Q^2 > 1$ GeV². The analysis of the lower Q^2 region down to about 0.3 GeV² is currently being finalized.

A comparison of the measured differential cross-section on carbon with the model predic-

tions (Sec. 3) is illustrated in Figure 5 for $E = 85$ GeV, indicating a good agreement in the entire kinematic region.

The NOMAD results are also consistent with the measurements performed by CHORUS and NuTeV on different targets [14]. Only in the recent NuTeV data a slight excess is observed for $x > 0.5$ [14]. The low Q^2 data from CHORUS support our treatment of the PCAC contribution to neutrino structure functions.

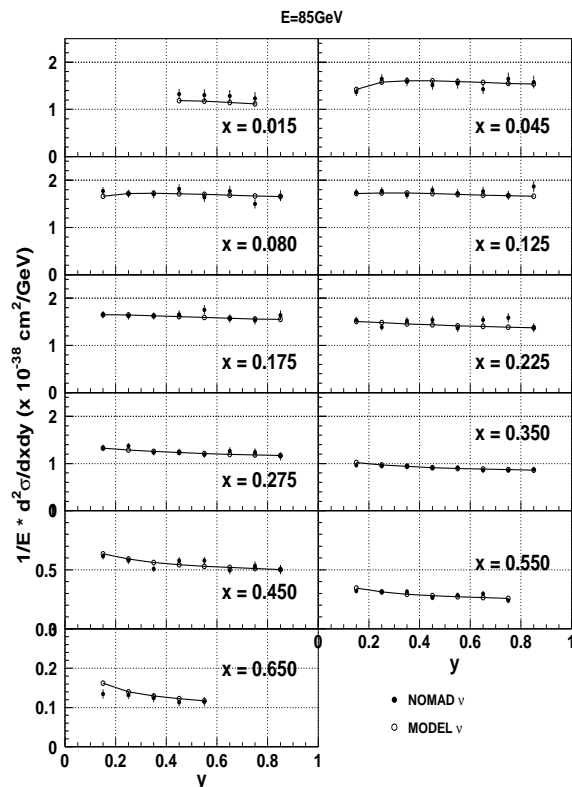


Figure 5. Differential neutrino CC cross-section on carbon at $E = 85$ GeV. The full circles show the NOMAD measurement while the curve with open circles is the prediction from our cross-section model.

5. Measurement of quasi-elastic cross-section

The reconstruction and identification of the recoiling proton track allows a measurement of the quasi-elastic cross-section $\nu_{\mu}n \rightarrow \mu^{-}p$ on carbon in NOMAD. A kinematic analysis based upon a three-dimensional likelihood function is used to reject backgrounds from DIS and resonance production. Overall, about 8000 two track events are selected for the cross-section determination in the energy range $3 < E_{\nu} < 100$ GeV. A complementary sample of about 16000 single track events is used as a cross-check of the reconstruction efficiency.

In order to reduce systematic uncertainties, NOMAD is measuring the ratio of quasi-elastic cross-section with respect to DIS ($W^2 > 4$ GeV²) processes. The absolute normalization is provided also in this case by the world average cross-section on isoscalar target.

The simulation of the quasi-elastic events is based upon the formalism by Llewellyn-Smith [26] and the axial form factor is parameterized in the conventional dipole form. Nuclear effects and the Pauli suppression factor are implemented following a simple Fermi gas model. Final state interactions are described by the DPMJET package [22]. The main systematic uncertainties are related to the understanding of nuclear corrections and are currently being finalized.

REFERENCES

1. P. Astier et al. *Nucl. Phys.* **B** 611, 3 (2001).
2. P. Astier et al. *Phys. Lett.* **B** 570, 19 (2003).
3. J. Altegoer et al. *Nucl. Instr. and Meth.* **A** 404, 96 (1998).
4. M. Anfreville et al. *Nucl. Instr. and Meth.* **A** 481, 339 (2002).
5. G. Bassompierre et al. *Nucl. Instr. and Meth.* **A** 403, 363 (1998); G. Bassompierre et al. *Nucl. Instr. and Meth.* **A** 411, 63 (1998).
6. D. Autiero et al. *Nucl. Instr. and Meth.* **A** 372, 556 (1996); D. Autiero et al. *Nucl. Instr. and Meth.* **A** 373, 358 (1996); D. Autiero et al. *Nucl. Instr. and Meth.* **A** 387, 352 (1997); D. Autiero et al. *Nucl. Instr. and Meth.* **A** 411, 285 (1998); D. Autiero et al. *Nucl. Instr. and Meth.* **A** 425, 188 (1999).
7. P. Astier et al. *Nucl. Instr. and Meth.* **A** 515, 800 (2003).
8. H. Georgi and H. D. Politzer, *Phys. Rev. D* **14**, 1829 (1976).
9. S.I. Alekhin, *Phys. Rev. D* **68** (2003) 014002, [arXiv:hep-ph/0211096].
10. S. Alekhin, S. Kulagin and R. Petti, paper in preparation.
11. S. Kulagin and R. Petti, *Nucl. Phys. A* 765, (2006) 126, [arXiv:hep-ph/0412425].
12. S. Kulagin and R. Petti, paper in preparation.
13. W. Melnitchouk, these proceedings.
14. S. Kulagin and R. Petti, these proceedings.
15. A. Arbuzov, D. Bardin and L. Kalinovskaya, hep-ph/0407203.
16. K. Diener, S. Dittmaier and W. Hollik, hep-ph/0310364.
17. A. Fasso, A. Ferrari, P. Sala and J. Ranft, Proceedings of the Monte Carlo 2000 Conference (Springer-Verlag, Berlin, 2001), 955.
18. G. Ingelman, LEPTO version 6.1, “The Lund Monte Carlo for Deep Inelastic Lepton-Nucleon Scattering”, TSL-ISV-92-0065 (1992); G. Ingelman, A. Edin, J. Rathsman, LEPTO version 6.5, *Comp. Phys. Comm.* **101** (1997) 108, [hep-ph/9605286].
19. T. Sjöstrand, “PYTHIA 5.7 and JETSET 7.4: physics and manual”, LU-TP-95-20 (1995), [arXiv:hep-ph/9508391]; T. Sjöstrand, *Comp. Phys. Comm* **39** (1986) 347, **43** (1987) 367.
20. GEANT : Detector Description and Simulation Tool, *CERN Programming Library Long Writup* **W5013**, GEANT version 3.21.
21. D. Rein and L. Sehgal, *Annals Phys.* 133, (1981) 79.
22. J. Ranft, *Phys. Rev. D* 51, (1995) 64; J. Ranft, arXiv:hep-ph/9911213.
23. A. Chukanov and R. Petti, in preparation.
24. M. Tzanov [NuTeV Collaboration], arXiv:hep-ex/0507040.
25. G. Öngüt *et al.* [CHORUS Collaboration], *Phys. Lett. B.* 632 (2006) 65.
26. C.L. Llewellyn-Smith, *Phys. Rep.* 3, (1972) 261.